

Metastable phase diagrams of Cu-based alloy systems with a miscibility gap in undercooled state

Chongde D. Cao · Zhanbo Sun · Xiaojun J. Bai ·
Libing B. Duan · Jianbang B. Zheng ·
Fang Wang

Received: 29 September 2010/Accepted: 6 May 2011/Published online: 25 May 2011
© Springer Science+Business Media, LLC 2011

Abstract Some Cu-based alloy systems with a large positive enthalpy of mixing display a eutectic or peritectic phase diagram under equilibrium conditions, but show a metastable liquid miscibility gap in the undercooled state. When the melt is undercooled below certain temperature beyond the critical liquid-phase separation temperature, it separates into two liquids with different compositions. The compositions of the two liquids change successively upon the metastable phase diagram before solidification occurs. The shape and position of the metastable miscibility gap are dependent of the alloy components and their interaction features. This study reviews the metastable phase diagrams of Cu-based alloy systems, which are derived from experiments and thermodynamic calculations.

Introduction

Some peritectic and eutectic alloys characterized by a large positive enthalpy of mixing show a miscibility gap in the metastable undercooled state. These alloys are mainly Cu-based, such as Cu–Co, Cu–Fe, Cu–Cr, Cu–Ta, Cu–Nb, Cu–Co–Fe, Cu–Co–Ni, etc. Nakagawa [1] firstly observed the metastable liquid-phase separation in Cu–Co and

Cu–Fe alloys when measuring their magnetic susceptibility during successive cooling. In the past several decades, two-liquid phase separation phenomena have been extensively investigated [2–7]. The metastable phase diagrams of the Cu–Co [8–13], Cu–Fe [14–22], Cu–Cr [23–34], and Cu–Nb [35–40] systems have been calculated and measured by many researchers. A miscibility gap in the undercooled Cu–Co–Fe alloys was observed using electromagnetic levitation technique [41]. The phase equilibria and the metastable immiscibility of this system were directly measured over a certain composition range and calculated [10, 42–47]. In addition, the metastable phase diagrams of some other ternary systems displaying a metastable miscibility gap have been studied [48–51]. So far, a considerable amount of work has been published on these alloy systems to assess the position of the miscibility gap. In this study, the metastable phase diagrams of the Cu-based alloy systems with a miscibility gap in undercooled state have been reviewed.

Metastable phase diagrams of binary alloy systems

Cu–Co system

Over the past decades, some researchers have accomplished a lot of research on the Cu–Co system. Munitz et al. [2, 3] investigated the Cu–Co alloys with a composition range of 33.3–89.3 at.% Cu and found an asymmetrical liquid-phase separation boundary. Robinson et al. [4] determined a symmetrical miscibility gap by pyrometric measurement on flux undercooled samples of compositions ranging from 18.9 to 92.1 at.% Cu. Using a similar flux method but using a thermocouple for temperature measurement, Yamauchi et al. [5] reported much lower

C. D. Cao (✉) · X. J. Bai · L. B. Duan · J. B. Zheng
Department of Applied Physics, Northwestern Polytechnical University, Xi'an 710072, China
e-mail: caocd@nwpu.edu.cn

Z. Sun
School of Science, Xi'an Jiaotong University,
Xi'an 710049, China

F. Wang
School of Computer Science and Technology, Northwestern Polytechnical University, Xi'an 710072, China

temperature values for liquid-phase separation of several Cu–Co alloys in the vicinity of the equiatomic composition. Letzig et al. [6] carried out electromagnetic levitation and drop tube experiments for Cu–Co alloys covering the composition range of 31–51 at.% Cu for considering metastable miscibility gap on the basis of analyzing the compositions of the separated majority and minority phases corresponding to different solidification temperatures. It is found that the phase separation and coagulation processes and microstructures are mainly controlled by the degree of undercooling, cooling rate, and convection level in the containerless states. A distorted microstructure is formed for Cu–Co alloys with near equiatomic compositions because of the electromagnetic stirring during electromagnetic levitation processing [6]. In contrast, disperse structures have been formed in droplets solidified during free fall in the drop tube [7, 8].

Cao et al. [7–9] successfully undercooled Cu–Co alloys over a composition range of 16.0–87.2 at.% Cu and directly measured the liquidus and critical liquid-phase separation temperatures using differential thermal analysis in combination with glass fluxing method. The directly determined miscibility gap boundary is slightly shifted to the Cu-rich side and basically symmetrical about 53 at.% Cu, with a quite flat dome. The critical temperature of liquid-phase separation is determined as 1547 K, which is about 108 K below the corresponding liquidus temperature and lower by about 32 K compared with most of the data

from previous investigations, as shown in Fig. 1. The calculated result based on a subregular solution model agrees well with the experimental data in this study. Palumbo et al. [10] performed an assessment of the binary Cu–Co systems using the CALPHAD approach, indicating that the critical point of the miscibility gap is 58.5 at.% Cu with a critical temperature of 1556 K and the minimum difference in temperature, 91 K, between the liquidus and the miscibility gap occurs at 67.5 at.% Cu. Curiotto et al. [11, 12] investigated several samples with different compositions by differential scanning calorimetry (DSC). High undercooling with respect to the liquidus was reached by means of the glass fluxing technique. The alloys were cycled with several heating and cooling runs for determining the temperature of liquid–liquid separation. For each composition, demixing and remixing temperatures were found to be equal. Zhao et al. [13] used a model to describe the kinetic details of the liquid–liquid decomposition during a cooling of the Cu–Co alloy in the metastable miscibility gap. This model has been applied for calculating the formation of the microstructure in the drop of the Cu–Co alloy. The calculated results have a good agreement with the experimental ones. The data of measured liquidus temperature, T_L , critical phase separation temperature, T_{sep} , and critical undercooling for phase separation, ΔT_{sep} , of Cu–Co alloys with various compositions from literatures are listed in Table 1.

Cu–Fe system

The phase diagram of the Cu–Fe system has been studied by many investigators [14–18]. There are three regions of primary solidification of the phase, ε , γ , and δ , within the system. The presence of two peritectic ($L + \delta \leftrightarrow \gamma$ and $L + \gamma \leftrightarrow \varepsilon$) and one eutectoid ($\gamma \leftrightarrow \varepsilon + \alpha$) transformations has been established. Measurements of the bimodal line have been carried out [1, 19, 20]. Immiscibility of liquid with an upper critical point of 1696 K at $x_{Fe} = 0.56$ was established by measuring the magnetic susceptibility of undercooled melts and microscopic analysis of quenched specimens [1]. Wilde et al. [19, 20] achieved a level of undercooling up to 250 K by the melt fluxing technique. In their study, apart from metastable immiscibility of the melt with a critical point of 1704 K at $x_{Fe} = 0.53$, the occurrence of a metastable solidification process $L \rightarrow \delta$ in the composition range $x_{Fe} = 0.43–0.96$ and a metastable syntectic transformation $L_1 + L_2 \leftrightarrow \varepsilon$ at 1405 K was observed. Turchanin and Agraval [21] calculated the parameters of stable and metastable phase equilibria of this system by means of the thermodynamic models. Figure 2 shows the phase diagram of the Cu–Fe alloy system with the measured [20] and calculated [18] metastable miscibility gap values. The data from literatures on measured

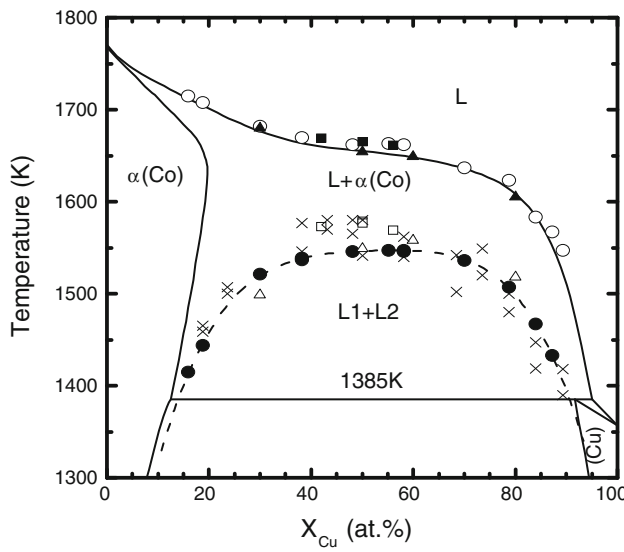


Fig. 1 Equilibrium phase diagram of the Co–Cu alloy system with the measured miscibility gap boundary according to different investigators: filled circle, Cao et al. [9]; open square, Nakagawa [1]; times symbols, Robinson et al. [4]; and open triangle, Yamauchi et al. [5], and the measured liquidus temperature by Cao et al. [9], open circle; Nakagawa [1], filled square; and Yamauchi et al. [5] filled triangle

Table 1 Measured liquidus temperature T_L , critical phase separation temperature T_{sep} , and critical undercooling for phase separation ΔT_{sep} of Cu–Co alloys with various compositions

Composition Cu–Co (at.%)	T_L (K)	T_{sep} (K)	ΔT_{sep} (K)	Experimental method	Reference
42–58	1669	1573	96	Magnetic susceptibility	[1]
50–50	1665	1579, 1577	86, 88	Magnetic susceptibility	[1]
56–44	1661	1569	92	Magnetic susceptibility	[1]
18.8–81.2	–	1459, 1465	–	DTA	[4]
23.6–76.4	–	1500, 1507	–	DTA	[4]
38.2–61.8	–	1546, 1577	–	DTA	[4]
43.1–56.9	–	1570, 1580	–	DTA	[4]
48.1–51.9	–	1565, 1580	–	DTA	[4]
50–50	–	1541, 1580	–	DTA	[4]
58.2–41.8	–	1540, 1562	–	DTA	[4]
68.4–31.6	–	1502, 1542	–	DTA	[4]
73.6–26.4	–	1520, 1549	–	DTA	[4]
78.8–21.2	–	1480, 1500	–	DTA	[4]
84.0–16.0	–	1419, 1447	–	DTA	[4]
89.3–10.7	–	1390, 1418	–	DTA	[4]
80–20	1605	1518	87	DTA	[5]
50–50	1654	1549	105	DTA	[5]
30–70	1680	1499	181	DTA	[5]
60–40	1649	1558	91	DTA	[5]
84–16	1583	1467	116	DTA	[7]
16.0–84.0	1713	1415	298	DTA	[9]
18.8–81.2	1708	1444	264	DTA	[9]
30.0–70.0	1682	1521	161	DTA	[9]
38.2–61.8	1669	1538	131	DTA	[9]
48.1–41.9	1661	1546	115	DTA	[9]
55.1–44.9	1664	1547	117	DTA	[9]
58.2–41.8	1662	1547	115	DTA	[9]
70.0–30.0	1636	1536	100	DTA	[9]
78.8–21.2	1623	1507	116	DTA	[9]
84.0–16.0	1582	1467	115	DTA	[9]
80–20	1612	1498	114	DSC	[11]
75–25	1650	1519	131	DSC	[11]
60–40	1653	1543	110	DSC	[11]
58.5–41.5	1657	1543	114	DSC	[11]
50–50	1664	1544	120	DSC	[11]
37–63	1672	1533	139	DSC	[11]
25–75	1690	1493	197	DSC	[11]
20–80	1706	1457	249	DSC	[11]
17–83	1708	1419	289	DSC	[11]
25–75	1691	1492	199	DSC	[12]
50–50	1666	1538	128	DSC	[12]
80–20	1609	1502	107	DSC	[12]

liquidus temperature critical phase separation temperature and critical undercooling for phase separation of Cu–Fe alloys are listed in Table 2.

The shape of the miscibility gap of the Cu–Fe system is similar to that of the Cu–Co system. Nevertheless, the

miscibility gap is only about 20 K below the liquidus line for the Cu–Fe system, implying that Cu–Fe alloys show a more intense tendency of demixing than Cu–Co alloys and so as to form egg-type structures in gas-atomized powders [22].

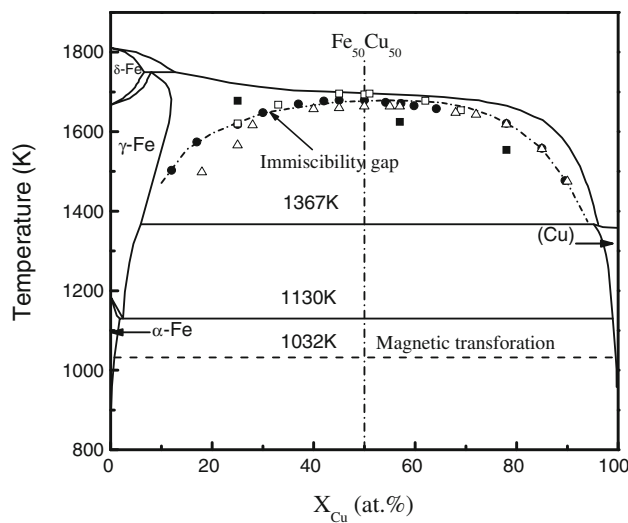


Fig. 2 Equilibrium phase diagram of the Cu–Fe alloy system with calculated [18] and measured metastable miscibility gap boundary according to different investigators: filled circle [20], open triangle [19], filled square [18], and open square [1]

Cu–Cr system

Cu–Cr alloys exhibit high mechanical strength and high electrical conductivity and therefore have been applied in electrical industries. In the early of last century, Hindrichs [23] pointed out that the Cu–Cr system is monotectic with a stable liquid miscibility gap between 42 and 94 at.%. Since then, some researchers have developed a similar type of phase diagram, and refined the boundary of the miscibility gap [24–26]. Meanwhile, however, a number of thermodynamic calculations predict that the binary Cu–Cr system

is eutectic, rather than monotectic [27–30]. Calculations also indicate that a metastable liquid miscibility gap develops immediately below the flat liquidus of Cr-rich solid solution. Chakrabarti and Laughlin [28] suggest that the metastable miscibility gap in undercooled liquid is probably stabilized by impurities under impure experimental conditions. Prompted by this hypothesis, Jacobs et al. [30] proposed a Cu–Cr phase diagram following a thermodynamic study of this system using the Knudsen cell-mass spectrometry. They calculated the metastable phase boundaries of this system, and predicted that the miscibility gap had a critical composition of 43.6 at.% Cr at 1787 K and expanded considerably at lower temperatures. Recently, some studies reported the formation of spherical Cr-rich grains in rapidly solidified Cu–Cr alloys with a high content of Cr [31–34]. Zhou et al. [32] investigated that the phase separation behavior in undercooled Cu–26.4 at.% Cr alloy melts using the electromagnetic levitation technique in combination with splat-quenching. During cooling, the solidification microstructures of levitated and splat-quenched samples are characterized by Cr-rich spheres in a Cu-rich matrix, showing clear evidence of metastable phase separation in the undercooled liquid. The liquid undercooling was estimated to be 210 K in terms of a newly calculated phase diagram. Recently, Gao et al. [33] investigated the microstructures of the Cu–Cr alloys containing 5–70 at.% Cr by electromagnetic levitation. It was found that the microstructures of the samples strongly depended on alloy composition. The alloys containing 5–60 at.% Cr showed a droplet-shaped microstructure, whereas those containing 65 and 70 at.% Cr displayed a banded microstructure. The observation of the

Table 2 Measured liquidus temperature T_L , critical phase separation temperature T_{sep} , and critical undercooling for phase separation ΔT_{sep} of Cu–Fe alloys with various compositions

Composition Cu–Fe (at.%)	T_L (K)	T_{sep} (K)	ΔT_{sep} (K)	Experimental method	Reference
25–75	1721	1621	100	Magnetic susceptibility	[1]
33–67	1719	1668	51	Magnetic susceptibility	[1]
45–55	1714	1696	18	Magnetic susceptibility	[1]
50–50	1715	1694	21	Magnetic susceptibility	[1]
51–49	1715	1696	19	Magnetic susceptibility	[1]
62–38	1701	1678	23	Magnetic susceptibility	[1]
69–31	1694	1654	40	Magnetic susceptibility	[1]
64.2–35.8	–	1658	–	DTA	[20]
59.8–40.2	–	1665	–	DTA	[20]
57.2–42.8	–	1671	–	DTA	[20]
54.2–45.8	–	1674	–	DTA	[20]
50–50	–	1679	–	DTA	[20]
45–55	–	1679	–	DTA	[20]
42–58	–	1677	–	DTA	[20]
37–63	–	1670	–	DTA	[20]
30–70	–	1648	–	DTA	[20]

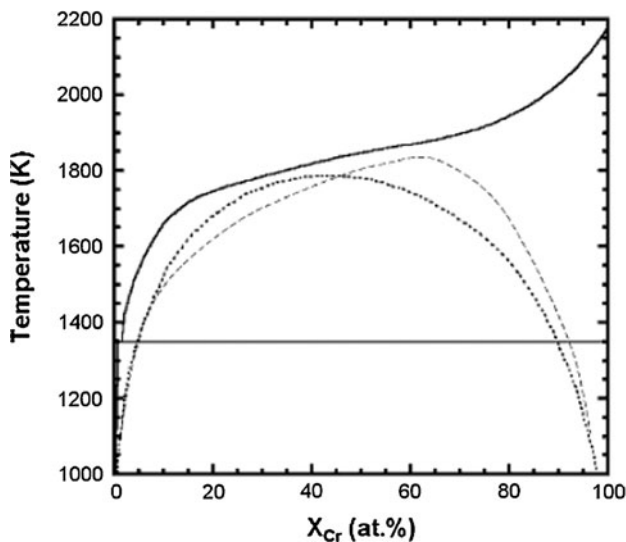


Fig. 3 Illustration of the metastable miscibility gap in the binary Cu–Cr system. The *dotted line* shows the prediction of the thermodynamic study by Jacobs et al. [30], whereas *dashed line* represents a hypothetical one based on the microstructure analysis by Zhou et al. [34]

two types of microstructures suggested the existence of a broad miscibility gap in the undercooled liquid. On the basis of these results, they estimated the metastable miscibility gap of Cu–Cr system, as shown in Fig. 3 on the basis of microstructure analysis [34], where the miscibility gap boundary shifted to the Cr-rich side.

Cu–Nb system

Cu–Nb alloys have attracted much interest because of their superconductivity and improved mechanical properties. Experimental and thermodynamic assessments of the Cu–Nb system have been carried out during the past few decades [35–38]. At present, there are two types of proposed phase diagrams for this system. Popov and Shiryaeva [35] suggested a stable liquid immiscibility phase diagram. In contrast, Allibert et al. [36] indicated horizontal liquidus but not immiscibility. Smith et al. [37] and Chakrabarti and Laughlin [38] concluded that the stable phase diagram of Cu–Nb should nearly have horizontal liquidus with a peritectic transformation. This nearly flat liquidus is indicative of a possible metastable liquid miscibility gap. Li et al. [39] determined accurate liquidus temperatures and examined the microstructures of the Cu–Nb alloys that were solidified in a very clean environment and at a low cooling rate. The Nb content for the alloys ranged from 3.4 to 80.7 at.%. They confirmed the equilibrium phase diagram having an S-shaped and nearly flat liquidus. Recently, Munitz et al. [40] used electromagnetic levitation to determine Cu–Nb phase diagram and to study supercooling effects on solidification characteristics of the Cu–Nb alloys

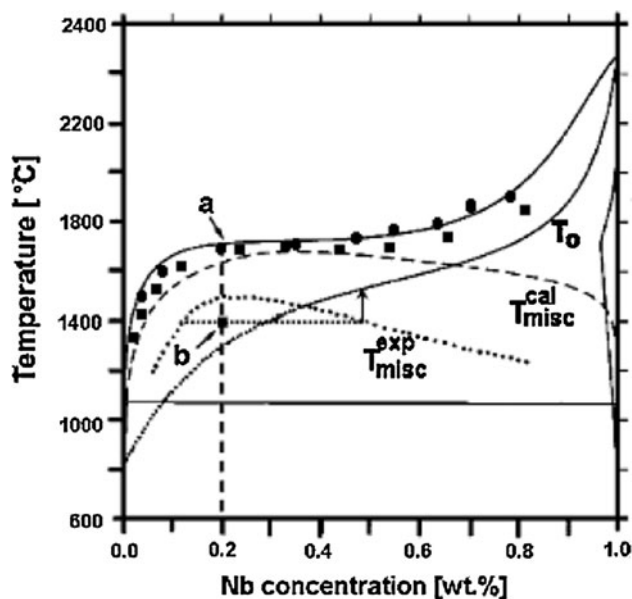


Fig. 4 Calculated stable phase diagram of Cu–Nb with calculated (*dashed line*) and experimentally suggested (*dotted line*) metastable liquid miscibility gap, as well as the calculated T_0 curve [40]. Superimposed are the data of measured liquidus temperature by Li et al. [39] (*filled square*) and Munitz et al. [40] (*filled circle*)

containing 3.4–61.4 at.% Nb. They found melt separation only for specimens containing approximately 14.6 at.% Nb. They gave a summary of measured liquidus temperatures of Cu–Nb alloys, as shown in Fig. 4. The calculated and experimentally suggested dome-shaped miscibility gap with a maximum of about 14.6 at.% Nb and the calculated T_0 curve are also presented.

Metastable phase diagrams of ternary alloy systems

When a third component is added into the above binary alloys characterized by liquid-phase separation in the undercooled state, the resulted ternary alloy system also shows a metastable miscibility gap over a certain composition range. The addition of the third component has different effects on the metastable liquid-phase separation behavior because of different interactions with the mother components. The metastable phase diagrams of some ternary systems have theoretically and experimentally been investigated, such as Cu–Co–Fe, Cu–Co–Ni, Cu–Cr–Ti, Cu–Cr–Zr, etc.

Cu–Co–Fe system

Jellinghaus [52] and Maddocks and Claussen [53] first investigated vertical sections of the phase diagram of Cu–Co–Fe ternary alloy system using thermal analysis and metallography, but they did not observe immiscibility

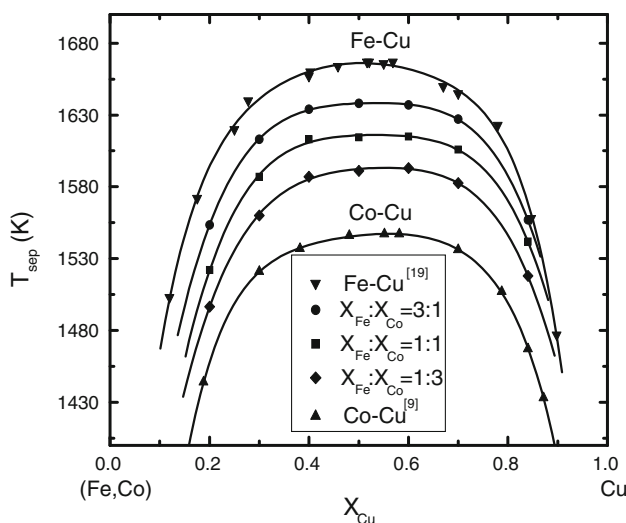


Fig. 5 Metastable miscibility gap boundaries of Cu–Co–Fe, Cu–Co, and Cu–Fe alloy systems [45]

behavior in this ternary system. Isothermal sections of the phase diagram at several temperatures had been obtained [54–56]. The involved both Cu–Co and Cu–Fe binary systems exhibit metastable liquid–liquid phase separation and therefore the Cu–Co–Fe ternary system must be characterized by a miscibility gap in the undercooling state. Munitz and Abbaschian [41] observed liquid-phase separation in Cu–Co–Fe alloys at high cooling rates. Kim and Abbaschian [42] measured the liquidus and demixing temperatures of some Cu–Co–Fe alloys by means of a pyrometer in the electromagnetic levitation state. Bamberger et al. [43] evaluated the stable and metastable Cu–Co–Fe phase diagrams. Wang et al. [44] calculated the phase equilibria in Cu–Fe–X (X: Co, Cr, Si, V) ternary systems and obtained the miscibility gaps theoretically. Cao and Görler [45] applied high-temperature differential thermal analysis and precisely determined the liquidus and the miscibility gap over a wide composition range for this system. The boundary lines of the miscibility gap, which are determined for the three quasi-binary cross sections of the Cu–(Fe,Co) alloy system, show remarkably flat domes. It is found that the directly determined miscibility gap boundary is quasi-binary at a given Cu concentration, which is located between the corresponding binodals of the boundary systems Cu–Co and Cu–Fe. The liquid-phase separation temperature determined directly and reproducibly from the onset temperature of the DTA traces, decreases monotonically with the increase of Co content, as shown in Fig. 5. Munitz et al. [46] used electromagnetic levitation to undercool the alloys and determined the metastable phase separation temperatures by analyzing the

compositions of the two separated liquids by EDS after solidification and compared with calculated data. Curiotto et al. [47] measured the temperatures of several selected Cu–Co–Fe alloys with different compositions by DSC. With a thorough SEM and EDS analysis of the samples, the effect of demixing and solidification on the formation of the microstructures had been disclosed with clear emphasis on the role of undercooling. The measured liquidus temperature, critical phase separation temperature, and critical undercooling for phase separation of Cu–Co–Fe alloys with various compositions are listed in Table 3.

On the basis of the experimental data available in the literatures, Palumbo et al. [10] calculated the Cu–Co–Fe phase diagram and obtained the metastable miscibility gap boundaries at various temperatures, as shown in Fig. 6. It is noteworthy that the miscibility gap does not present a sharp saddle point in the middle of the phase diagram, as obtained in the assessment by Wang et al. [22]. This is mainly because of the new description of the binary Cu–Co system, where the maximum of the miscibility gap occurs at a lower temperature.

Cu–Co–Ni system

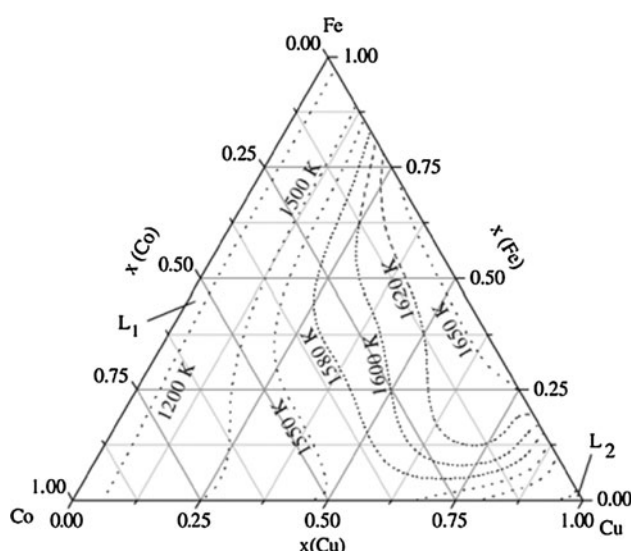
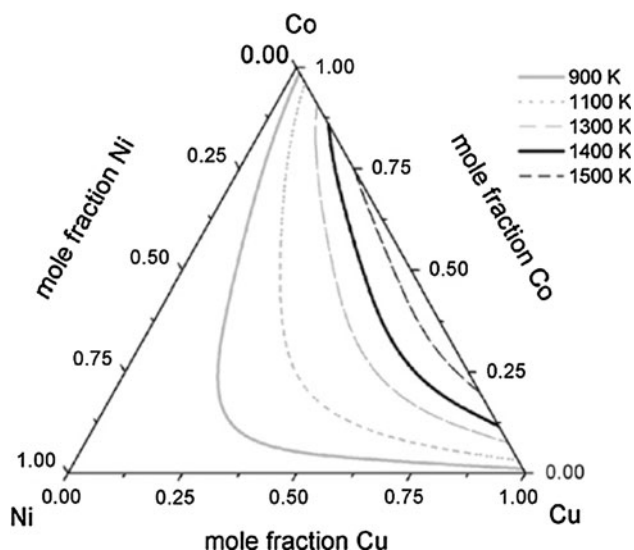
It is found that adding Ni to Cu–Co can partly restrain the liquid-phase separation and can decrease the volume fraction of Co-rich particles in the Cu-rich matrix [48]. Waehlert and Oster [57] employed thermal analysis for investigating the liquidus curve of Cu–Co–Ni. A more extensive investigation was carried out in [58], where 90 alloys were investigated to determine 11 vertical sections of the Cu–Co–Ni phase diagram. More recently, Hasebe et al. [59] studied the phase equilibria of Cu–Co–Ni alloys at temperatures between 1150 and 1550 K using the diffusion couple technique. They also calculated the ternary phase diagrams but without considering the liquid-phase separation. Curiotto et al. [49] measured the transformation temperatures of Cu–Co–Ni alloys by DSC in combination with glass fluxing. On the basis of the experimental data obtained, evaluation of the Cu–Co–Ni ternary system was carried out, where, in particular, attention had been paid to the description of the metastable liquid miscibility gap, as shown in Fig. 7. Table 4 lists the measured liquidus temperature, critical phase separation temperature, and critical undercooling for phase separation of some Cu–Co–Ni alloys. It was found that Ni additions reduce the demixing temperature, leading to the binodal line below the peritectic. Only the demixing occurring at high temperatures (curves close to the Cu–Co side) is experimentally accessible, and that calculated at low temperatures should be considered with caution because of extrapolation.

Table 3 Measured liquidus temperature T_L , critical phase separation temperature T_{sep} , and critical undercooling for phase separation ΔT_{sep} of Cu–Co–Fe alloys with various compositions

Composition (at.%) Cu–Co–Fe	T_L (K)	T_{sep} (K)	ΔT_{sep} (K)	Experimental method	Reference
37–11–50	1668	1627	41	EML	[42]
36–22–42	1665	1622	43	EML	[42]
36–33–31	1395	1342	53	EML	[42]
36–44–20	1400	1330	70	EML	[42]
36–54–10	1396	1318	78	EML	[42]
47–11–42	1388	1365	23	EML	[42]
46–23–31	1389	1356	33	EML	[42]
46–33–21	1397	1351	46	EML	[42]
46–44–21	1394	1340	54	EML	[42]
56–12–32	1384	1352	32	EML	[42]
56–23–31	1392	1347	45	EML	[42]
55–34–11	1386	1337	49	EML	[42]
66–12–22	1371	1336	35	EML	[42]
66–23–11	1353	1329	24	EML	[42]
77–12–11	1322	1298	24	EML	[42]
10–45–45	1727	No sep.	–	DTA	[45]
20–20–60	1711	1553.5	158	DTA	[45]
20–40–40	1696	1522.5	173.5	DTA	[45]
20–60–20	1693	1496.5	196.5	DTA	[45]
25.7–45–29.3	1677	1558	119	DTA	[45]
30–17.5–52.5	1695	1613	82	DTA	[45]
30–52.5–17.5	1678	1560	118	DTA	[45]
40–15–45	1688	1634	54	DTA	[45]
40–30–30	1675	1613	62	DTA	[45]
40–45–15	1668	1587	81	DTA	[45]
50–12.5–37.5	1685	1638	47	DTA	[45]
50–37.5–12.5	1663	1591	72	DTA	[45]
60–10–30	1667	1637	30	DTA	[45]
60–20–20	1662	1615	47	DTA	[45]
60–30–10	1656	1593	63	DTA	[45]
70–7.5–22.5	1689	1627	62	DTA	[45]
70–15–15	1656	1606	50	DTA	[45]
70–22.5–7.5	1650	1582.5	67.5	DTA	[45]
75–10–15	1664	1600	64	DTA	[45]
75–15–10	1648	1586	62	DTA	[45]
84–4–12	1623	1557	66	DTA	[45]
84–8–8	1619	1542	77	DTA	[45]
84–12–4	1616	1518	98	DTA	[45]
81.6–8.4–10	1513	1412	101	EML	[46]
72.9–10.5–16.6	1553	1468	85	EML	[46]
69.5–5.2–25.3	1563	1523	40	EML	[46]
62.9–26.1–11.0	1563	1513	50	EML	[46]
57.5–20.7–21.8	1573	1423	50	EML	[46]
52.7–31.0–16.3	1603	1553	50	EML	[46]
52.1–10.2–37.7	1626	1586	40	EML	[46]
46.7–16.4–36.9	1613	1588	25	EML	[46]
44.7–36.9–18.4	1598	1528	70	EML	[46]
90–5–5	1577	1456	121	DSC	[47]

Table 3 continued

Composition (at.%) Cu–Co–Fe	T_L (K)	T_{sep} (K)	ΔT_{sep} (K)	Experimental method	Reference
50–25–25	1669	1618	51	DSC	[47]
50–12.5–37.5	1687	1637	50	DSC	[47]
50–37.5–12.5	1670	1591	79	DSC	[47]
25–30–45	1693	1569	124	DSC	[47]
25–65–10	1688	1514	174	DSC	[47]
25–10–65	1711	1601	110	DSC	[47]
12–22–66	1727	1444	283	DSC	[47]
12–44–44	1715	—	—	DSC	[47]

**Fig. 6** Calculated metastable miscibility gap boundaries at various temperatures of the Cu–Co–Fe system [10]**Fig. 7** Calculated metastable miscibility gap boundaries of Cu–Co–Ni system at different temperatures [49]

Cu–Cr–Zr and Cu–Cr–Ti systems

Figure 8a,b exhibits the projections of the metastable miscibility gap boundaries at various temperatures of the Cu–Cr–Zr and Cu–Cr–Ti ternary systems, which were calculated on the basis of the subregular solution model by Sun et al. [50, 51]. These phase diagrams show the effect of Ti and Zr addition on the liquid-phase separation of Cu–Cr alloys. It is revealed that the addition of Ti or Zr can partly suppress the liquid-phase separation of the Cu–Cr alloy melts, resulting in refining of Cr-rich particles formed after liquid-phase separation during rapid cooling. The thermodynamic analyses indicate that the large positive heat of mixing between Cu and Cr is reduced by the addition of Ti and Zr, leading to the liquid-phase separation occurring at a lower temperature and being driven by a smaller force.

Key factors controlling the formation of the metastable liquid miscibility gap

From the insight of thermodynamics, an alloy melt can be treated as a subregular solution. The Gibbs free energy of mixing G_{mix} of a binary alloy melt derives from ideal entropy of mixing and the excess free energy

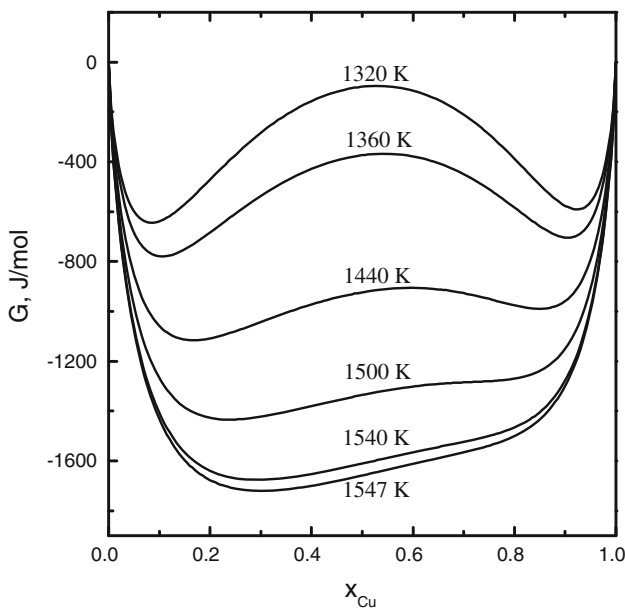
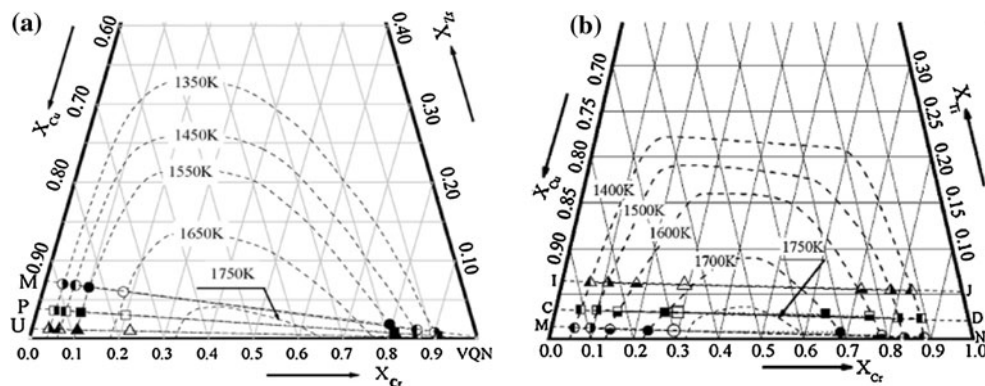
$$G_{mix} = RT(X_A \ln X_A + X_B \ln X_B) + \Omega_{AB}X_AX_B \quad (1)$$

where Ω_{AB} is the interaction parameter between the components A and B. This parameter is dependent on composition and temperature. For binary Cu–Co system, the Gibbs free energy of mixing dependent on composition and temperature is shown in Fig. 9. Below the critical liquid-phase separation temperature, 1547 K, there exist two minima in the Gibbs free energy of mixing, leading to the occurrence of liquid-phase separation. The interaction parameters of the Cu–Co and Cu–Fe systems are different. This causes different critical liquid-phase separation temperatures and corresponding compositions for these systems.

In the case of a ternary system, the Gibbs free energy of mixing can be expressed as

Table 4 Measured liquidus temperature T_L , critical phase separation temperature T_{sep} , and critical undercooling for phase separation ΔT_{sep} of Cu–Co–Ni alloys with various compositions

Composition Cu–Co–Ni (at.%)	T_L (K)	T_{sep} (K)	ΔT_{sep} (K)	Experimental method	Reference
49–49–2	1653	1521	132	DSC	[49]
47.5–47.5–2	1655	1482	173	DSC	[49]
46–46–8	1653	1448	205	DSC	[49]
44.5–44.5–11	1643	1412	231	DSC	[49]
43–43–15	1644	1372	272	DSC	[49]
80–15–5	1559	1386	173	DSC	[49]
22.5–72.5–5	1691	1426	265	DSC	[49]

Fig. 8 Calculated metastable miscibility gap boundaries of Cu–Cr–Zr [50] (a) and Cu–Cr–Ti [51] systems (b)**Fig. 9** Gibbs free energy of mixing of Cu–Co system at various temperatures as a function of composition

$$\begin{aligned} G_{\text{mix}} = & RT(X_A \ln X_A + X_B \ln X_B + X_C \ln X_C) \\ & + \Omega_{AB} X_A X_B + \Omega_{AC} X_A X_C + \Omega_{BC} X_B X_C \\ & + \Omega_{ABC} X_A X_B X_C \end{aligned} \quad (2)$$

where Ω_{ABC} is the interaction parameters of A–B–C. This means that the excess free energy is dependent not only on the interaction parameters of A–B, A–C, and B–C, but also on that of A–B–C. Both Cu–Co and Cu–Fe systems exhibit positive enthalpy of mixing, but the Co–Fe is thermodynamically an ideal mixing system. The critical temperature of the Cu–Co–Fe system increases with the increase of Fe content. In contrast, the Cr–Ti(Zr) and Cu–Ti(Zr) are the systems with negative enthalpy of mixing. The increase of Ti(Zr) content could decrease the enthalpy of mixing, resulting in significant suppression of metastable liquid-phase separation in the Cu–Cr–Ti or Cu–Cr–Zr ternary systems.

From the insight of physics, the bond fraction among different components in an alloy melt is related to the interaction among the components. A lower fraction of bonds among different components implies weaker interaction among these different components, resulting in more intensive tendency of liquid-phase separation. In sum, the interaction among components is the dominant factor controlling the formation of metastable liquid miscibility gap.

Conclusion

The large positive enthalpy of mixing results in immiscibility in some Cu-based peritectic and eutectic alloys in the

undercooling state. So far, the metastable phase diagram is mainly derived from thermodynamic calculation, where the interaction parameters among the involved elements are the key factors. Composition analysis on the solidified-separated phases, direct measurement on a levitated drop by a infrared pyrometer, DSC, and differential thermal analysis techniques have been employed to experimentally determine the metastable miscibility gap. Evidently, the thermal analysis in combination with glass fluxing method can lead to the most accurate data because the liquid–liquid phase separation process causes a very small temperature change. So far, extensive research has been done on the binary alloy systems. In contrast, however, only a little information is available for the metastable phase diagram of multicomponent alloy systems. From the insight of thermodynamics and physics, it is inferred the interaction among components is the dominant factor controlling the formation of metastable liquid miscibility gap.

Acknowledgements The authors are grateful to Mr. Jing Wang and Mr. Xiang Zeng for their help. This study was financially supported by the National Natural Science Foundation of China (Grant Nos. 50871088 and 50871081), the Natural Science Foundation of Shaanxi, the International Cooperation Program of Shaanxi, and Specialized Research Fund for the Doctoral Program of Higher Education.

References

- Nakagawa Y (1958) Acta Metall 6:704
- Munitz A, Elder SP, Abbaschian R (1992) Metall Trans 23A:1817
- Munitz A, Abbaschian R (1996) Metall Mater Trans A 27A:4049
- Robinson MB, Li D, Rathz TJ, Williams G (1999) J Mater Sci 34:3747. doi:[10.1023/A:1004688313591](https://doi.org/10.1023/A:1004688313591)
- Yamauchi I, Ueno N, Shimaoka M, Ohnaka I (1998) J Mater Sci 33:371. doi:[10.1023/A:1004319829612](https://doi.org/10.1023/A:1004319829612)
- Letzig T, Cao CD, Bender W, Kolbe M, Herlach DM (2000) Mat-wissuwerkstofftechnik 31:825
- Cao CD, Herlach DM, Kolbe M, Gorler GP, Wei B (2003) Scr Mater 48:5
- Cao CD, Herlach DM, Wei B (2002) J Mater Sci Lett 21:341
- Cao CD, Gorler GP, Herlach DM, Wei B (2002) Mater Sci Eng A325:503
- Palumbo M, Curiotto S, Battezzati L (2006) Calphad 30:171
- Curiotto S, Pryds NH, Johnson E, Battezzati L (2007) Mater Sci Eng A449–451:644
- Curiotto S, Greco RH, Pryds N, Johnson E, Battezzati L (2007) Fluid Phase Equilib 256:132
- Zhao JZ, Kolbe M, Li HL, Gao JR, Ratke L (2007) Metall Mater Trans A 38A:1162
- Lindqvist PA, Uhrénus B (1980) Calphad 3:193
- Chuang YY, Schmid R, Chang YA (1984) Metall Trans A 15:1921
- Lu XY, Cao CD, Wei B (2001) Mater Sci Eng A313:198
- Hasebe M, Nishizawa T (1980) Calphad 4:83
- Oikamoto H (1993) Phase diagram of binary iron alloys. ASM International, Materials Park, OH, pp 131–137
- Wilde G, Willnecker R, Singh RN, Sommer F (1997) Z Metallkd 88:804
- Wilde G, Perepezko JH (1999) Acta Mater 47:3009
- Turchanin MA, Agraval PG (2001) Powder Metall Met Ceram 40:7
- Wang CP, Liu XJ, Ohnuma I, Kainuma R, Ishida K (2002) Science 9:990
- Hindrichs G (1908) Z Anorg Chem 59:415
- Siedschlag E (1923) Z Anorg Chem 131:173
- Leonov M, Bochvar N, Ivanchenko V, Nauk D (1986) Akad SSSR 290:888
- Müller R (1988) Siemens Forsch u Entwickl Ber 17:105
- Kuznetsov GM, Fedorov VN, Rodnyanskaya AL (1977) Sov Non-Ferrous Met Res 3:104
- Chakrabarti DJ, Laughlin DE (1984) Bull Alloy Phase Diagrams 5:59
- Zeng K, Hämäläinen M (1995) Calphad 19:93
- Jacobs KT, Priya S, Waseda Y (2000) Z Metallkd 91:594
- Sun ZB, Zhang C, Zhu Y, Yang Z, Ding B, Song X (2003) J Alloys Compd 361:165
- Zhou ZM, Wang YP, Gao J, Kolbe M (2005) Mater Sci Eng A398:318
- Gao J, Wang YP, Zhou ZM, Kolbe M (2007) Mater Sci Eng A449–451:654
- Zhou ZM, Gao J, Li F, Zhang YK, Wang YP, Kolbe M (2009) J Mater Sci 44:3793. doi:[10.1007/s10853-009-3511-y](https://doi.org/10.1007/s10853-009-3511-y)
- Popov IA, Shiryaeva NV (1961) Russ J Inorg Chem 6:1184
- Allibert C, Driole J, Bonnier E (1969) Acad Sci Paris 268C:1579
- Smith JF, Lee KJ, Baily DM (1984) Bull Alloy Phase Diagrams 5:1984
- Chakrabarti DJ, Laughlin DE (1982) Bull Alloy Phase Diagrams 2:455
- Li D, Robinson MB, Rathz TJ (2000) J Phase Equilib 2:2000
- Munitz A, Bamberger M, Venkert A, Landau P, Abbaschian R (2009) J Mater Sci 44:64. doi:[10.1007/s10853-008-3115-y](https://doi.org/10.1007/s10853-008-3115-y)
- Munitz A, Abbaschian R (1998) J Mater Sci 33:3639. doi:[10.1023/A:1004663530929](https://doi.org/10.1023/A:1004663530929)
- Kim DI, Abbaschian R (2000) J Phase Equilib 21:25
- Bamberger M, Munitz A, Kaufman L, Abbaschian R (2002) Calphad 26:375
- Wang CP, Liu XJ, Ohnuma I, Kainuma R, Ishida K (2002) J Phase Equilib 23:236
- Cao CD, Görler GP (2005) Chin Phys Lett 22:482
- Munitz A, Bamberger AM, Wannaparhun S, Abbaschian R (2006) J Mater Sci 41:2749. doi:[10.1007/s10853-006-5598-8](https://doi.org/10.1007/s10853-006-5598-8)
- Curiotto S, Battezzati L, Johnson E, Palumbo M, Pryds N (2008) J Mater Sci 43:3253. doi:[10.1007/s10853-008-2540-2](https://doi.org/10.1007/s10853-008-2540-2)
- Sun ZB, Song X, Hu Z, Yang S, Liang G, Cochrane R (2001) J Alloys Compd 319:276
- Curiotto S, Battezzati L, Johnson E, Pryds N (2007) Acta Mater 55:6642
- Sun ZB, Guo J, Li Y, Zhu YM, Li Q, Song XP (2008) Metall Mater Trans A 39A:1054
- Sun ZB, Guo J, Song XP, Zhu YM, Li Y (2008) J Alloys Compd 455:243
- Jellinghaus W (1936) Archiv fur das Eisenhuettenwesen 10:115
- Maddocks WR, Claussen GE (1936) Iron and Steel Institute, London, Special Report 14:116
- Oikawa K (1981) Thesis of Master of Engineering. Tohoku University, Japan
- Jiang M, Hao SM (1990) In: Proceedings of the 6th national symposium on phase diagram, p 150
- Ohtani H, Suda H, Ishida K (1997) ISIJ Int 37:207
- Waehlert M, Oster Z (1914) Berg Huttenwesen 62:357
- Dannoh V, Neumann H (1938) Z Metallkd 30:217
- Hasebe M, Oikawa K, Nishizawa T (1982) Jpn Inst Met 46:584